An H_∞ Controller With Wind Disturbance Rejection Properties for the DSS-13 Antenna

W. Gawronski
Communications Ground Systems Section

The feed-forward and linear quadratic Gaussian (LQG) controllers significantly reduced the servo error at higher rate tracking. However, the servo error due to wind disturbances acting on the antenna structure is still significant. This error cannot be reduced by the feed-forward controller and is only moderately reduced by the LQG controller. The H_∞ *controller design approach gives the possibility of addressing the problems of command following and disturbance rejection. The* H_∞ *controller that was designed for the DSS-13 antenna improves the tracking performance of the existing LQG controller and significantly reduces the servo error due to wind disturbances. The antenna model, as well as the wind model, were obtained from the field tests rather than from analysis, which increases confidence in the simulation results.*

I. Introduction

The baseline servo configuration of the DSS-13 antenna includes the proportional and integral (PI) controller. This controller was upgraded recently with the addition of the feed-forward (FF) loop (see [1]) and of the linear quadratic Gaussian (LQG) controller (see [2] and [3]). The basic purpose of the FF controller is to reduce tracking error at high rates. It is used for rates ranging from 0.1 to 4 deg/s. However, the FF controller excites flexible deformation of the antenna if the command accelerations are excessive. On the other hand, the LQG controller not only reduces the tracking error at higher rates but also suppresses antenna vibrations even for significant command accelerations.

A significant portion of the tracking error is generated by the antenna vibrations excited by wind gusts. Although the pointing error caused by the wind-induced antenna dynamics is a concern, there was not a direct effort to design a controller that would reduce the action of wind disturbances. The addition of the FF controller neither improves nor weakens the wind disturbance rejection properties of the baseline PI controller. The LQG controller improves tracking, but its disturbance rejection properties were not addressed in the design process, and therefore, they are rather moderate. The H_∞ controller has the inherent possibility of customizing its properties so that its tracking and the disturbance rejection properties are addressed simultaneously. In this article, the design of the H_∞ controller is presented. The design results are illustrated with the simulation results of command following (e.g., step input) and with the tracking simulations in a 50-km/h wind.

II. The H_∞ Controller Structure

The closed-loop system architecture is shown in Fig. 1, where G is the transfer function of a plant, K is the transfer function of a controller, w is the exogenous input (commands and disturbances), u is the actuator input, z is the regulated output (at which performance is evaluated), and y is the sensed output.

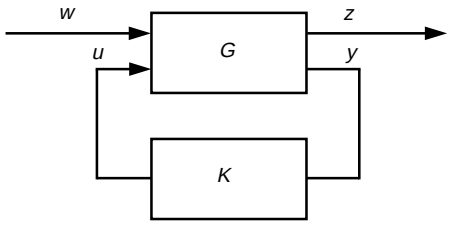

Fig. 1. The closed-loop system configuration.

A. Problem Definition

The H_∞ control problem consists of determining the controller K such that the H_∞ norm of the closed-loop transfer function G_{zw}, from w to z, is minimized over all realizable controllers K; that is, one has to find realizable K such that

$$||G_{zw}(K)||_\infty \tag{1}$$

is minimal. The plant transfer function $G(s)$ and the controller transfer function $K(s)$ are such that

$$\left.\begin{aligned} \begin{pmatrix} z(s) \\ y(s) \end{pmatrix} &= G(s) \begin{pmatrix} w(s) \\ u(s) \end{pmatrix} \\ u(s) &= K(s)y(s) \end{aligned}\right\} \tag{2}$$

In the related state–space equations

$$\left.\begin{aligned} \dot{x} &= Ax + B_1 w + B_2 u \\ z &= C_1 x + D_{12} u \\ y &= C_2 x + D_{21} w \end{aligned}\right\} \tag{3}$$

(A, B_2) is stabilizable and (A, C_2) is detectable. We will design a so-called central H_∞ controller, for which the conditions

$$\left.\begin{aligned} D_{12}^T \begin{bmatrix} C_1 & D_{12} \end{bmatrix} &= \begin{bmatrix} 0 & I \end{bmatrix} \\ D_{21} \begin{bmatrix} B_1^T & D_{21}^T \end{bmatrix} &= \begin{bmatrix} 0 & I \end{bmatrix} \end{aligned}\right\} \tag{4a}$$

are satisfied. Additionally, the matrices

$$\left.\begin{array}{l} \begin{bmatrix} A - j\omega I & B_2 \\ C_1 & D_{12} \end{bmatrix} \\ \\ \begin{bmatrix} A - j\omega I & B_1 \\ C_2 & D_{21} \end{bmatrix} \end{array}\right\} \tag{4b}$$

have full column rank (see [4] and [5]). Let G_{zw} be the transfer function of the closed-loop system from w to z. Then there exists an admissible controller such that $||G_{zw}|| < \rho$, where ρ is the smallest number such that the following four conditions hold:

(1) $S_{\infty c} \geq 0$ solves the following central Riccati equation:

$$S_{\infty c}A + A^T S_{\infty c} + C_1^T C_1 - S_{\infty c}\left(B_2 B_2^T - \rho^{-2} B_1 B_1^T\right) S_{\infty c} = 0 \tag{5a}$$

(2) $S_{\infty e} \geq 0$ solves the following central Riccati equation:

$$S_{\infty e}A^T + A S_{\infty e} + B_1 B_1^T - S_{\infty e}\left(C_2^T C_2 - \rho^{-2} C_1^T C_1\right) S_{\infty e} = 0 \tag{5b}$$

(3) The inequality

$$\lambda_{\max}(S_{\infty c} S_{\infty e}) < \rho^2 \tag{5c}$$

holds, where $\lambda_{\max}(X)$ is the largest eigenvalue of X.

(4) The Hamiltonian matrices

$$\begin{bmatrix} A & \rho^{-2} B_1 B_1^T - B_2 B_2^T \\ -C_1^T C_1 & -A^T \end{bmatrix}$$
$$\begin{bmatrix} A^T & \rho^{-2} C_1^T C_1 - C_2^T C_2 \\ -B_1 B_1^T & -A \end{bmatrix} \tag{5d}$$

do not have eigenvalues on the $j\omega$ axis.

With the above conditions satisfied, the controller realization $(A_\infty, B_\infty, C_\infty)$, from input y to output u, is given as

$$\left.\begin{array}{l} A_\infty = A + \rho^{-2} B_1 B_1^T S_{\infty c} + B_2 k_c + k_e C_2 \\ \\ B_\infty = -k_c \\ \\ C_\infty = k_e \end{array}\right\} \tag{6a}$$

where

$$\left.\begin{aligned} k_c &= -B_2^T S_c \\ k_e &= -S_o S_\infty e C_2^T \\ S_o &= \left(I - \rho^{-2} S_{\infty e} S_{\infty c}\right)^{-1} \end{aligned}\right\} \tag{6b}$$

The gain k_c is called the controller gain, while the gain k_e is the filter (estimator) gain. Note that the form of the solution is similar to the LQG solution. However, the LQG gains are determined independently, while the H_∞ gains are coupled through Inequality (5c) and the component S_o. The size of the controller is equal to the size of the plant.

Balanced coordinates are used for the controller design. An H_∞ controller is balanced if the related solutions of Eqs. 5(a) and 5(b) are equal and diagonal, i.e., if

$$\left.\begin{aligned} S_{\infty c} &= S_{\infty e} = M_\infty \\ M_\infty &= \mathrm{diag}\left(\mu_{\infty 1}, \mu_{\infty 2}, \ldots, \mu_{\infty N}\right) \end{aligned}\right\} \tag{7}$$

$\mu_{\infty 1} \geq \mu_{\infty 2} \geq \cdots \geq \mu_{\infty N} > 0$, where $\mu_{\infty i}$ is the ith H_∞ characteristic (or singular) value.

The transformation R_∞ to this representation is determined as follows: Let

$$\left.\begin{aligned} P_{\infty c} &= S_{\infty c}^{1/2} \\ P_{\infty e} &= S_{\infty e}^{1/2} \end{aligned}\right\} \tag{8a}$$

denote $N_\infty = P_{\infty c} P_{\infty e}$, and let

$$N_\infty = V_\infty M_\infty U_\infty^T \tag{8b}$$

be the singular value decomposition of N_∞. For the transformation R_∞,

$$R_\infty = P_{\infty e} U_\infty M_\infty^{-1/2} = P_{\infty c}^{-1} V_\infty M_\infty^{1/2} \tag{9}$$

of the state x such that $\overline{x} = R_\infty x$, the representation $(R_\infty^{-1} A R_\infty, R_\infty^{-1} B_1, R_\infty^{-1} B_2, C_1 R_\infty, C_2 R_\infty)$ is H_∞ balanced.

B. Closed-Loop System Equations

The state–space equations of the open-loop system follow from Eq. (3):

$$\left.\begin{aligned} \dot{x} &= Ax + B_1 w + B_2 u \\ z &= C_1 x + D_{12} u \\ y &= C_2 x + D_{21} w \\ u &= k_c \hat{x} \end{aligned}\right\} \tag{10a}$$

and the state–space equations of the central H_∞ controller are as follows (see [4] and [5]):

$$\dot{\hat{x}} = \left(A + k_e C_2 + \rho^{-2} B_1 B_1^T S_{\infty c} + B_2 k_c\right) \hat{x} - k_e y \tag{10b}$$

where

$$\left.\begin{aligned} k_c &= -B_2^T S_{\infty c} \\ k_e &= -S_o S_{\infty e} C_2^T \\ S_o &= \left(I - \rho^{-2} S_{\infty e} S_{\infty c}\right)^{-1} \end{aligned}\right\} \tag{11}$$

Defining a new state variable $x_o^T = [x^T \quad e^T]$, where $e = x - \hat{x}$, one obtains the closed-loop state–space equations

$$\left.\begin{aligned} \dot{x}_o &= A_o x_o + B_o w \\ z &= C_o x_o \end{aligned}\right\} \tag{12a}$$

where

$$A_o = \begin{bmatrix} A + B_2 k_c & -B_2 k_c \\ -\rho^{-2} B_1 B_1^T S_{\infty c} & A + k_e C_2 + \rho^{-2} B_1 B_1^T S_{\infty c} \end{bmatrix} \tag{12b}$$

$$B_o = \begin{bmatrix} B_1 \\ B_1 - k_c D_{21} \end{bmatrix} \tag{12c}$$

$$C_o = [C_1 + D_{12} k_c \quad -D_{12} k_c] \tag{12d}$$

The block diagram of the closed-loop system is shown in Fig. 2.

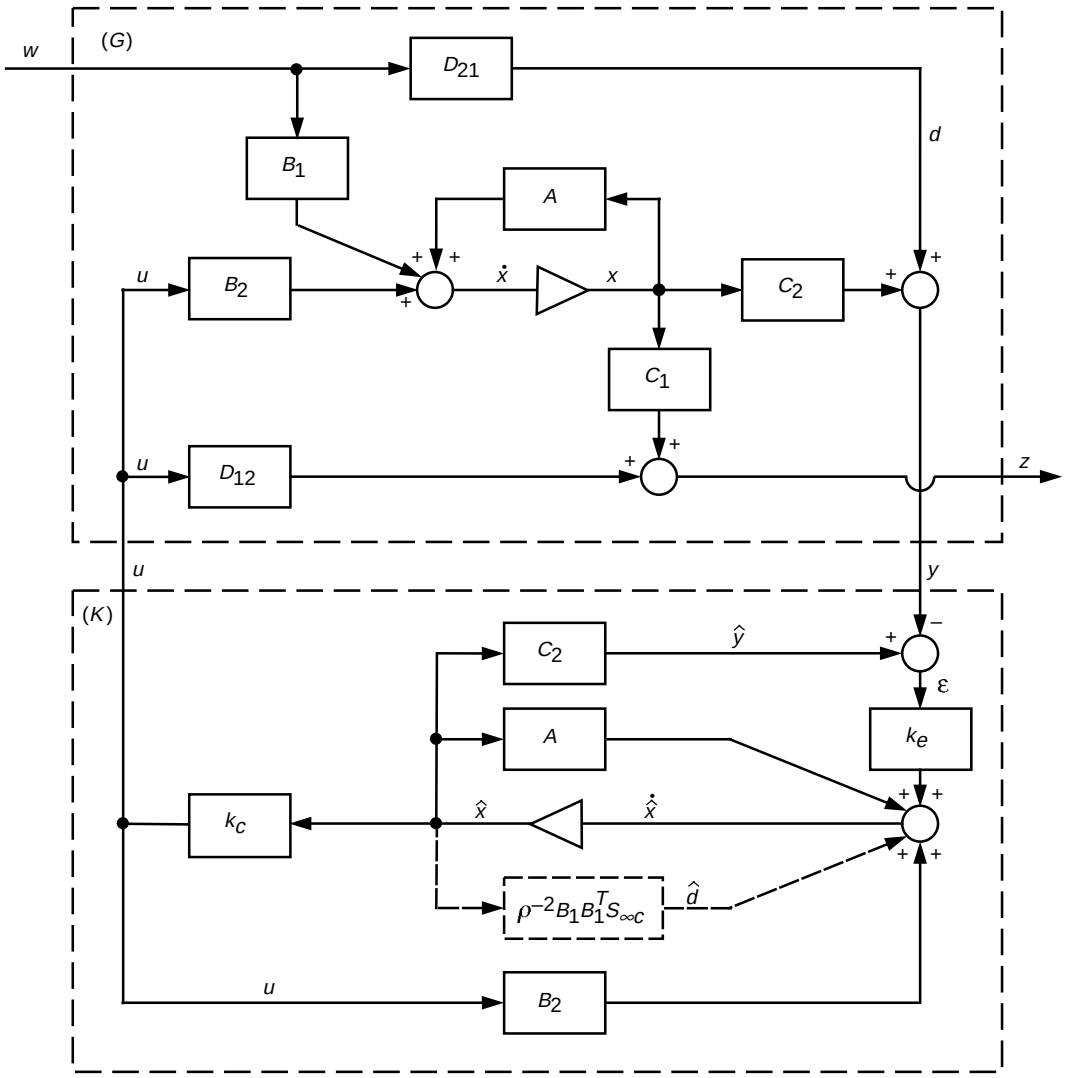

Fig. 2. The H_∞ closed-loop system.

For the balanced H_∞ system, one obtains from Eq. (11)

$$\left.\begin{aligned} k_c &= -B_2^T M_\infty \\ k_e &= -S_o M_\infty C_2^T \\ S_o &= \left(I - \rho^{-2} M_\infty^2\right)^{-1} \end{aligned}\right\} \tag{13a}$$

or, denoting $k_c = [k_{c1}, \ldots, k_{cn}]$, $k_e^T = [k_{e1}^T, \ldots, k_{en}^T]$, $B_2^T = [B_{21}^T, \ldots, B_{2n}^T]$, and $C_2 = [C_{21}, \ldots, C_{2n}]$, then

$$\left.\begin{aligned} k_{ci} &= -\mu_{\infty i} B_{2i}^T \\ k_{ei} &= -\mu_{\infty i} s_{oi} C_{21} \\ s_{oi} &= \frac{\rho^2}{\rho^2 - \mu_{\infty i}^2} \end{aligned}\right\} \tag{13b}$$

C. The Tracking H_∞ Controller

The tracking controller performance depends not only on the plant parameters, but also on the tracking command profile (its rate, acceleration, etc.). One important requirement for tracking systems is to maintain zero steady-state error. This requirement can be satisfied by upgrading the plant with an integrator. An H_∞ tracking controller with an integral upgrade is presented in Fig. 3.

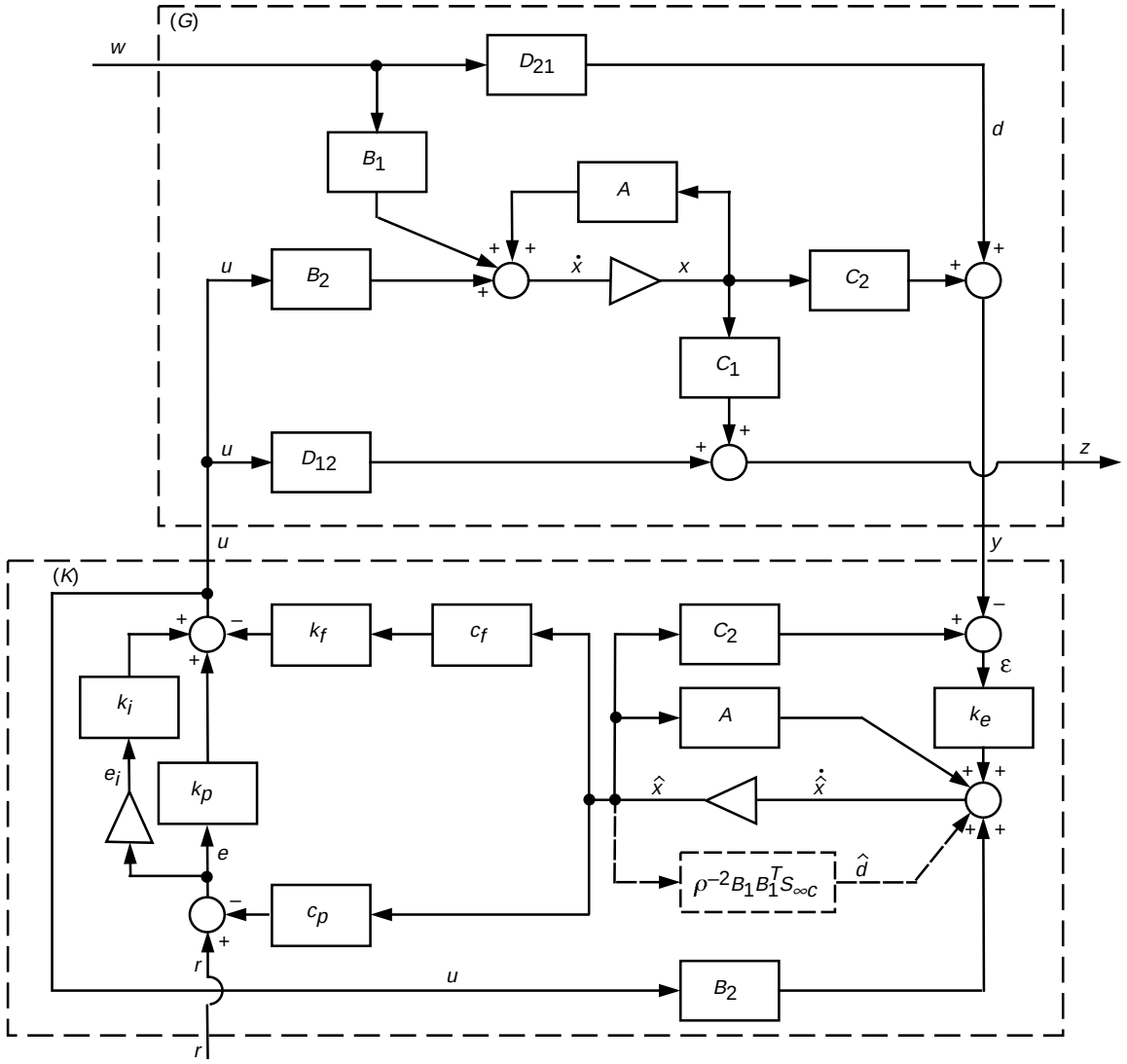

Fig. 3. The H_∞ tracking controller with an integral upgrade.

D. Choosing the H_∞ Controller Structure To Be Identical With the LQG Controller

Comparing the H_∞ controller structure, as in Fig. 3, with the LQG controller structure, as in [2] and [6], one can see that they are identical except for an additional feedback with the gain $\rho^{-2}B_1B_1^TS_{\infty c}$ in the H_∞ controller (shown as a dashed line in Figs. 2 and 3). This gain can be avoided in order to keep the same structure of the control software. This is done by assuming very large ρ. For the following reason, this should not dramatically change the closed-loop system performance: It can be seen from Eq. (13b) that the estimator gain (k_{ei}) depends on ρ and that $k_{e1} \to \infty$ as $\rho \to \mu_{\infty 1}$, but the increase of the gain k_{e1} will not greatly improve the system performance. Denote $\varepsilon_1 = \rho^2 - \mu_{\infty 1}^2$, and as ε_1 approaches zero, the performance, measured by $||G_{zw}||_\infty$, improves negligibly, although the gain increase is of the order ε_1^{-2}.

E. Wind Filter Shaping

In [7], the wind filter was determined from the wind field data. Its state–space model has to be added to the loop model, and the complexity of the plant increases. However, if the rate loop model is in the balanced representation, the filter addition can be simplified, as shown in the Appendix, by appropriate scaling of the input matrix B of the rate loop model. The scaling factors are the filter gains at the natural frequencies of the antenna.

III. Simulation Results

The controllers for the azimuth and elevation axes were simulated separately. In these simulations, the antenna model, [3], as well as the wind model, [7], were obtained from the field tests rather than from analysis. The data-based model increases confidence in the simulation results.

A. The Azimuth Axis Controller

The PI controller performance has been described in [8]. The LQG design, as in [2] and [3], is already implemented at the DSS-13 antenna. Its proportional gain is $k_p = 12$, and the integral gain is $k_i = 10$. The tracking performances of both controllers are evaluated with their transfer functions in Fig. 4. The plots show significantly improved tracking performance of the LQG controller (the bandwidths are 0.08 and 1.2 Hz for the PI and LQG controllers, respectively). The wind gust simulation results are shown in Table 1. The wind disturbance rejection improvement of the LQG controller (or H_∞ controller) with respect to the PI controller is evaluated with the coefficient β, which is defined as the ratio of the rms servo errors:

$$\beta = \frac{\sigma_X}{\sigma_{PI}} \tag{14}$$

where σ_X is the rms servo error of either the LQG or H_∞ controller and σ_{PI} is the rms error of the PI controller.

The simulation shows that the LQG controller, when compared with the PI controller, significantly improves antenna tracking performance and slightly improves the wind disturbance rejection properties (the servo error in wind was reduced by 13 percent, i.e., $\beta = 0.87$). This result illustrates the need for a new controller with the improved disturbance rejection properties.

Two designs of the H_∞ controller are now discussed and compared with the performance of the PI and LQG control system. The first H_∞ controller design is such that it preserves the tracking part of the LQG controller (hence its proportional gain is chosen to be the same as the LQG proportional gain, $k_p = 12$, and the integral gain is chosen to be the same as the LQG integral gain, $k_i = 10$). However, the other gains (k_f and k_e) were modified to improve the disturbance rejection properties. The simulation results

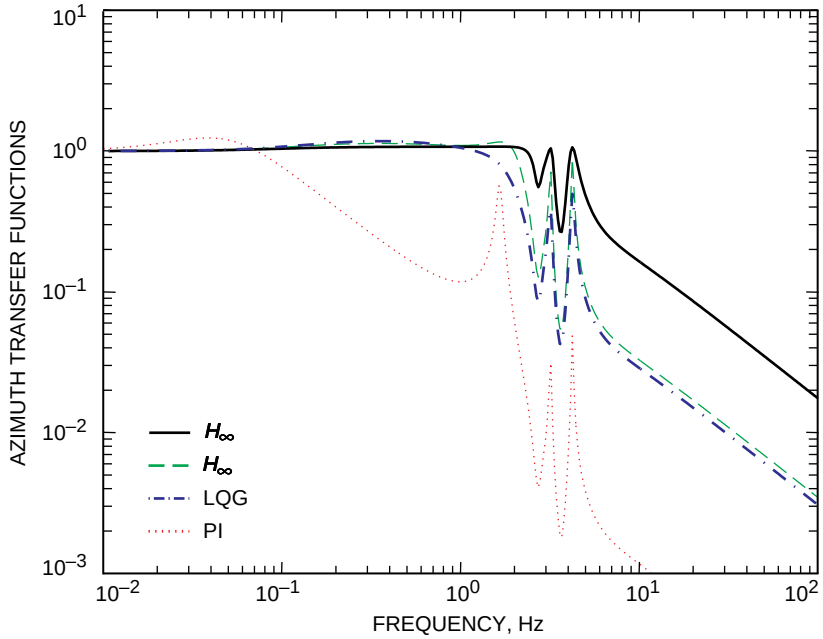

Fig. 4. Magnitudes of the azimuth transfer functions of the PI, LQG, and first and second H_∞ controllers.

Table 1. DSS-13 azimuth servo error in 50-km/h gusts.

Controller	RMS servo error, mdeg	Performance, β	Bandwidth, Hz
PI	0.8	1	0.08
LQG	0.7	0.87	1.2
H1	0.4	0.50	2.0
H2	0.13	0.17	2.4

(the transfer functions in Fig. 4) show a slight tracking improvement of the H_∞ controller in comparison with the LQG controller (a 2-Hz bandwidth versus a 1.2-Hz bandwidth). The wind servo error (rms) has been reduced significantly, from 0.8 to 0.4 mdeg (see Table 1).

The second H_∞ design was intended to obtain the best wind disturbance rejection properties while preserving the tracking properties. The H_∞ design gave increased PI gains. This can be explained by the fact that the large portion of the wind disturbances includes low-frequency spectra (below 1 Hz), and this bandwidth is predominantly governed by the proportional and the integral gains. These gains were increased to $k_p = 70$ and $k_i = 40$. The tracking performance is illustrated with the magnitude of the transfer function in Fig. 4. The bandwidth of the second H_∞ controller increased to 2.4 Hz. The azimuth servo error due to wind gusts is shown in Fig. 5. This error decreased significantly, to 0.13 mdeg. It is a 6 times reduction in comparison with the PI controller.

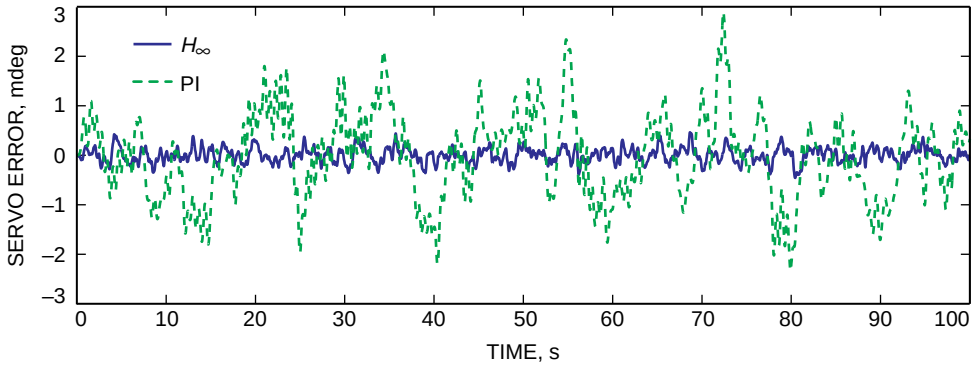

Fig. 5. The azimuth servo error due to wind gusts.

B. Elevation Axis Controller Simulations

The structure of the elevation axis controller is the same as the azimuth axis controller. Again, we tested two H_∞ controller designs, one with the tracking part similar to the LQG controller and the second with the enhanced tracking/disturbance properties. The results are summarized in Table 2. The tracking performances of the elevation axis controllers are evaluated with their transfer functions in Fig. 6. It shows the expanding bandwidth from the PI to the LQG, to the first H_∞, and to the second H_∞ controllers. The disturbance rejection properties of the elevation LQG controller were compared with those of the PI. These properties are better than those of the azimuth LQG controller; from Table 2, it can be seen that the servo error due to 50-km/h wind gusts dropped over 3 times. Moreover, the servo error for the first H_∞ controller was 6 times smaller than that of the PI controller, and the second H_∞ controller was 18 times smaller (see Fig. 7). At the same time, the bandwidth of the H_∞ controllers expanded to 2.8 Hz.

Table 2. DSS-13 elevation servo error in 50-km/h gusts.

Controller	RMS servo error, mdeg	Performance, β	Bandwidth, Hz
PI	7.5	1	0.08
LQG	2.2	0.30	2.2
H1	1.3	0.17	2.3
H2	0.4	0.06	2.8

IV. Conclusions

The new controllers for the DSS-13 antenna have been designed and analyzed. The design based on the H_∞ approach shows improved tracking performance. For example, the H_∞ closed-loop bandwidth increased significantly as compared with the LQG controller (not to mention the PI controller). More importantly, the wind disturbance rejection properties improved, since the rms servo errors of the H_∞ controller dropped significantly as compared with the rms errors of the PI and LQG controllers. The improvement is achieved through the determination of the H_∞ controller's parameters. The presented H_∞ design preserves the existing LQG controller structure. Therefore, its implementation can be achieved without structural modifications of the software, and no new hardware is necessary.

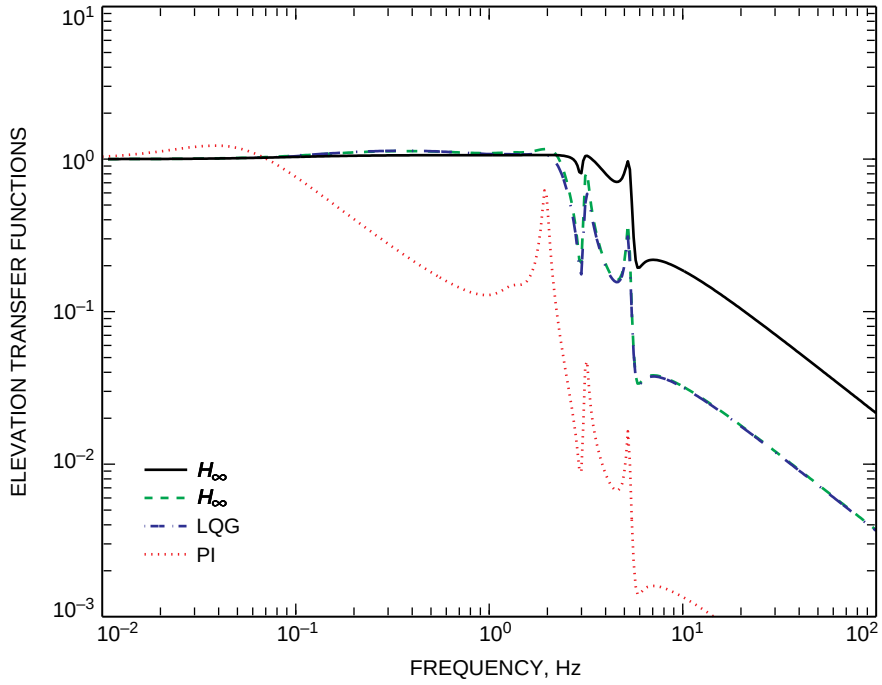

Fig. 6. Magnitudes of the elevation transfer functions of the PI, LQG, and the first and second H_∞ controllers.

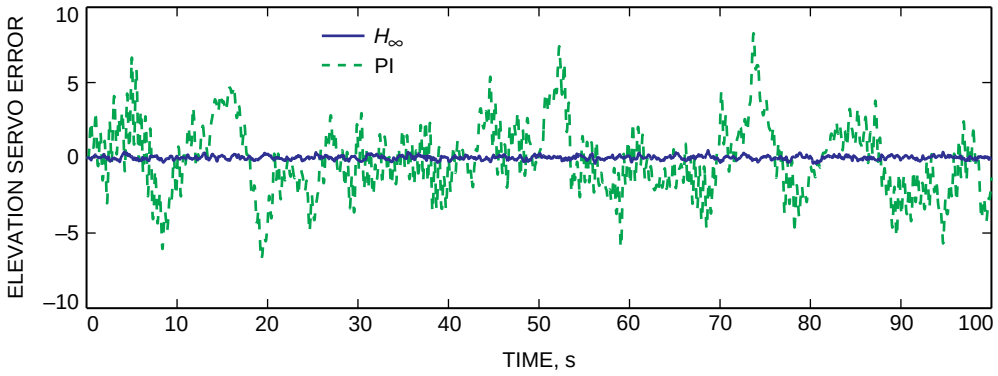

Fig. 7. The elevation servo error due to wind gusts.

The main concern is the robustness of the H_∞ controller. Its performance was achieved by narrowing its tolerance to the antenna parameter variations. The variations occur with the elevation angle changes. An in-field robustness check will follow, and a compromise between robustness and performance will be achieved.

Based on the current analysis, one can expect significant improvement in the suppression of wind disturbances.

References

[1] "Feed-Forward Control Upgrade of the Deep Space Network Antennas," *The Telecommunications and Data Acquisition Progress Report 42-110, April–June 1992*, Jet Propulsion Laboratory, Pasadena, California, pp. 253–262, August 15, 1992.

[2] W. Gawronski, "Design of the Reduced LQG Compensator for the DSS-13 Antenna," *The Telecommunications and Data Acquisition Progress Report 42-112, October–December 1992*, Jet Propulsion Laboratory, Pasadena, California, pp. 83–106, February 15, 1993.

[3] W. Gawronski, C. S. Racho, and J. A. Mellstrom, "Application of the LQG and Feedforward Controllers to the Deep Space Network Antennas," *IEEE Trans. on Control System Technology*, vol. 3, pp. 417–421, 1995.

[4] J. C. Doyle, K. Glover, P. P. Khargonekar, and B. A. Francis, "State Space Solutions to Standard H^2 and H_∞ Control Problems," *IEEE Trans. Automatic Control*, vol. 34, pp. 831–847, 1989.

[5] K. Glover and J. C. Doyle, "State-Space Formulae for All Stabilizing Controllers That Satisfy an H-norm Bound and Relations to Risk Sensitivity," *Systems and Control Letters*, vol. 11, pp. 167–172, 1988.

[6] W. Gawronski and J. A. Mellstrom, "Control and Dynamics of the Deep Space Network Antennas," in *Control and Dynamics Systems*, edited by C. T. Leondes, vol. 63, San Diego, California: Academic Press, pp. 289–412, 1994.

[7] W. Gawronski, "Wind Gust Models Derived From Field Data," *The Telecommunications and Data Acquisition Progress Report 42-123, July–September 1995*, Jet Propulsion Laboratory, Pasadena, California, pp. 30–36, November 15, 1995. http://tda.jpl.nasa.gov/tda/progress_report/42-123/123G.pdf

[8] W. Gawronski and J. A. Mellstrom, "Modeling and Simulations of the DSS 13 Antenna Control System," *The Telecommunications and Data Acquisition Progress Report 42-106, April–June 1991*, Jet Propulsion Laboratory, Pasadena, California, pp. 205–248, August 15, 1991.

[9] W. Gawronski, *Balanced Control of Flexible Structures*, London: Springer, 1996.

[10] K. B. Lim, P. G. Maghami, and S. M. Joshi, "Comparison of Controller Designs for an Experimental Flexible Structure," *IEEE Control System Magazine*, pp. 108–118, June 1992.

Appendix
Wind Filter Implementation

It will be shown that the addition of a filter in the H_∞ design is equivalent to the multiplication of each row of the plant input matrix B by a constant. The ith constant is the filter gain at the ith natural frequency of the structure.

I. Flexible Structure Properties

The antenna rate-loop model is in the H_∞ balanced representation. Its transfer function G has the state representation (A, B, C). In this case, the system matrix $A(n \times n)$ is block diagonally dominant [9], with 2×2 blocks on the diagonal, and B and C are divided into $2 \times n_d$ and $n_d \times 2$ blocks ($n_d = n/2$):

$$\left.\begin{aligned} A &\simeq \mathrm{diag}(A_i) \\ B &= \begin{bmatrix} B_1 \\ B_2 \\ \vdots \\ B_{n_d} \end{bmatrix} \\ C &= \begin{bmatrix} C_1 & C_2 & \cdots & C_{n_d} \end{bmatrix} \end{aligned}\right\} \tag{A-1a}$$

where

$$A_i = \begin{bmatrix} -\zeta_i\omega_i & \omega_i \\ -\omega_i & -\zeta_i\omega_i \end{bmatrix} \tag{A-1b}$$

and ζ_i is the ith modal damping. Denote

$$\left.\begin{aligned} G_i &= C_i(j\omega I - A_i)^{-1}B_i \\ G &= C(j\omega I - A)^{-1}B \end{aligned}\right\} \tag{A-2}$$

Then, for the above representation, one obtains

$$G \simeq \sum_{i=1}^{n_d} G_i \tag{A-3}$$

and

$$G(\omega_i) \simeq G_i(\omega_i) \tag{A-4}$$

II. Closed-Loop Design

For the closed-loop design, the plant transfer function G includes two inputs, the exogenous input w (that includes commands and disturbances) and the actuator input u, and two outputs, the regulated output z (at which performance is evaluated) and the sensed output y. The transfer function of a controller is K. Denote G_f the transfer function of the input filter; then the transfer function G_{fzw} from w to z with the input filter is

$$G_{fzw} = G_{zw}G_f \tag{A-5}$$

III. Frequency Weighting for the H_∞ Controller

Frequency weighting of the exogenous inputs and regulated outputs is a standard procedure in the H_∞ design for obtaining the required closed-loop properties (see, for example, [10]). In this case, a plant is augmented with the input and/or output shaping filters, forming a new plant model that is consequently used in the controller design. For wind disturbance modeling purposes, we consider the input shaping only.

In this case, the norm $||G_{fzw}||_\infty$ rather than $||G_{zw}||_\infty$ is minimized. Let (A_{zw}, B_{zw}, C_{zw}) be the H_∞ state–space representation of G_{zw} and (A_f, B_f, C_f) be the state–space representation of G_f. Using Eqs. (A-3) and (A-4), one obtains

$$||G_{fzw}||_\infty = ||G_{zw}G_f||_\infty \simeq \max_i ||G_{zwi}G_f(\omega_i)||_\infty = \alpha_{fi} \max_i ||G_{zwi}||_\infty \tag{A-6}$$

where

$$\alpha_{fi} = |G_f(\omega_i)| \tag{A-7}$$

and ω_i is the ith natural frequency. Thus, the weighting impacts the transfer functions only at the natural frequencies of the structure.

In this case, Eq. (A-6) can be rewritten as follows:

$$||G_{fzw}||_\infty = \max_i ||\alpha_{fi}C_{zw}(j\omega I - A_{zw})^{-1}B_{zw}||_\infty \tag{A-8}$$

Thus,

$$||G_{fzw}||_\infty \simeq ||G_{zwo}||_\infty \tag{A-9}$$

where

$$G_{zwo} = C_{zw}(j\omega I - A_{zw})^{-1}B_{zwo} \tag{A-10a}$$

$$B_{zwo} = \alpha_f B_{zw} \tag{A-10b}$$

or

$$B_{zwoi} = \alpha_{fi} B_{zwi} \tag{A-10c}$$

and

$$\alpha_f = \text{diag}(\alpha_{fi}), \quad i = 1, 2, \ldots, n_d \tag{A-10d}$$

Equations (A-9) and (A-10) show that the application of the input filter for the H_∞ performance modeling is equivalent to the scaling of the $2 \times n_d$ blocks of input matrix B_{zw} with scalars α_{fi}. The scalar α_{fi} is the magnitude of the filter transfer function at the resonant frequency ω_i [see Eq. (A-7)].